

Supplementary information

**Enhancing electrochemical methane coupling in solid oxide cells by tuning oxygen
species in the catalyst**

Xiaoyong Xu *^{a1}, Haobo Li ^{a1}, Xu Han^a, Yao Zheng *^a

^a School of Chemical Engineering, The University of Adelaide, SA 5005, Australia.

* E-mail: xiaoyong.xu@adelaide.edu.au; yao.zheng01@adelaide.edu.au;

¹ These authors contributed equally to this work.

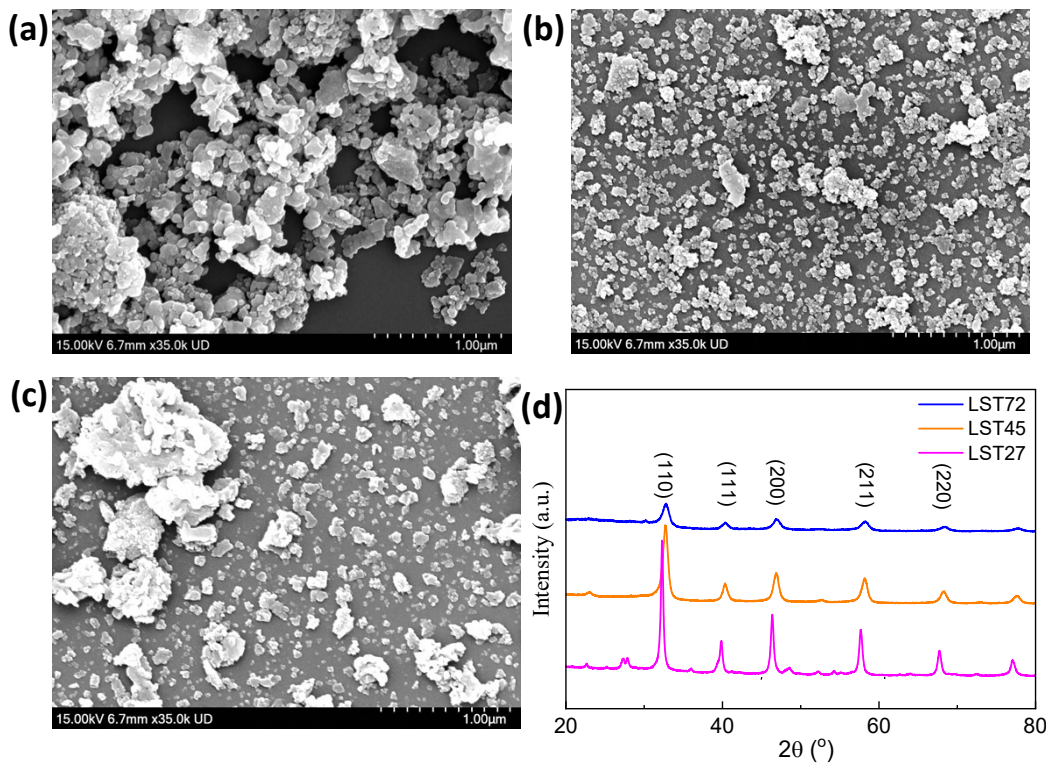


Fig. S1 Morphology of LST powder (a) LST27; (b) LST45; (c) LST72; (d) XRD patters for LST.

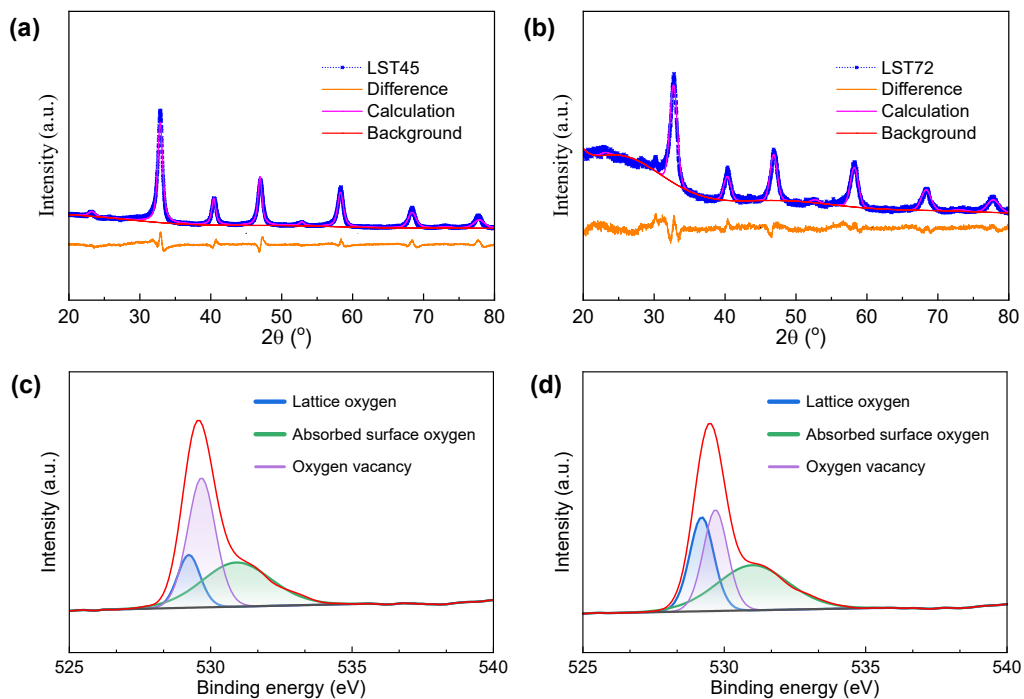


Fig. S2 X-ray diffraction Rietveld refinements of LST powder (a) LST45; (b) LST72; XPS for LST (c) LST45; (d) LST72.

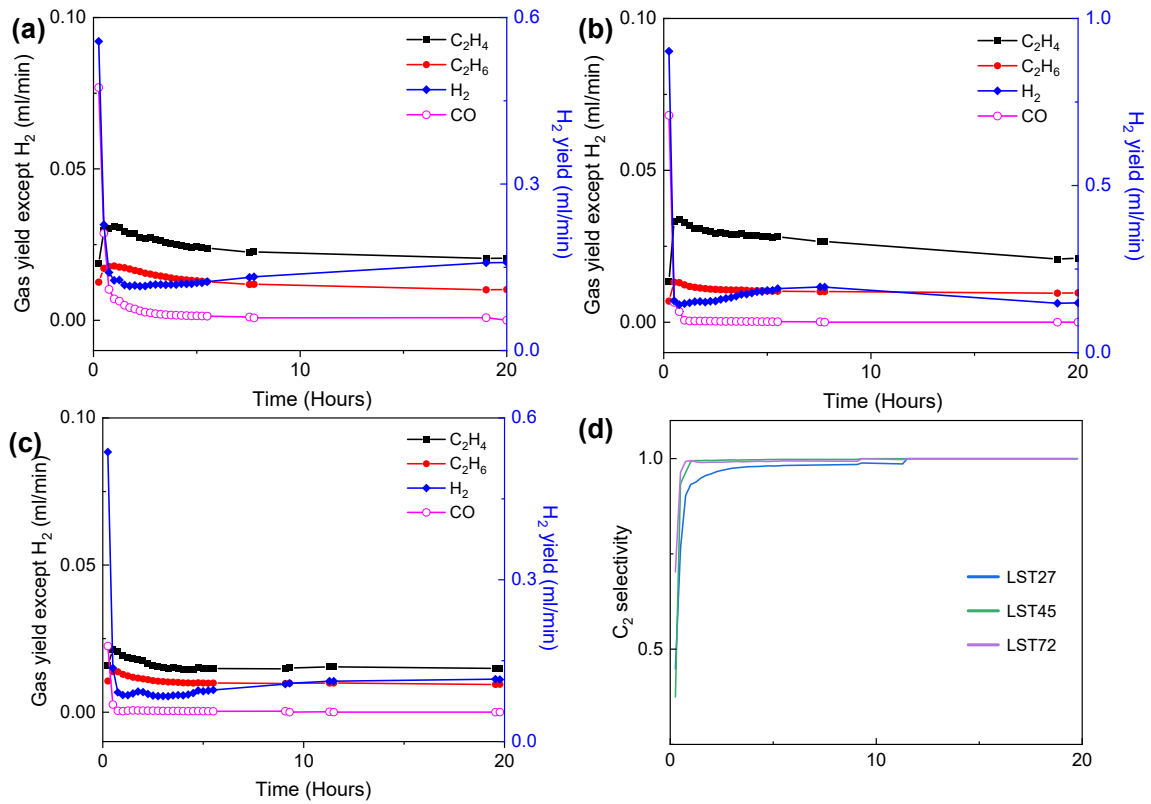


Fig. S3 Total concentration of hydrogen and CO during nonoxidative methane coupling at 850 °C with (a)LST27GDC; (b)LST45GDC; (c)LST72GDC; (d) C₂ selectivity.

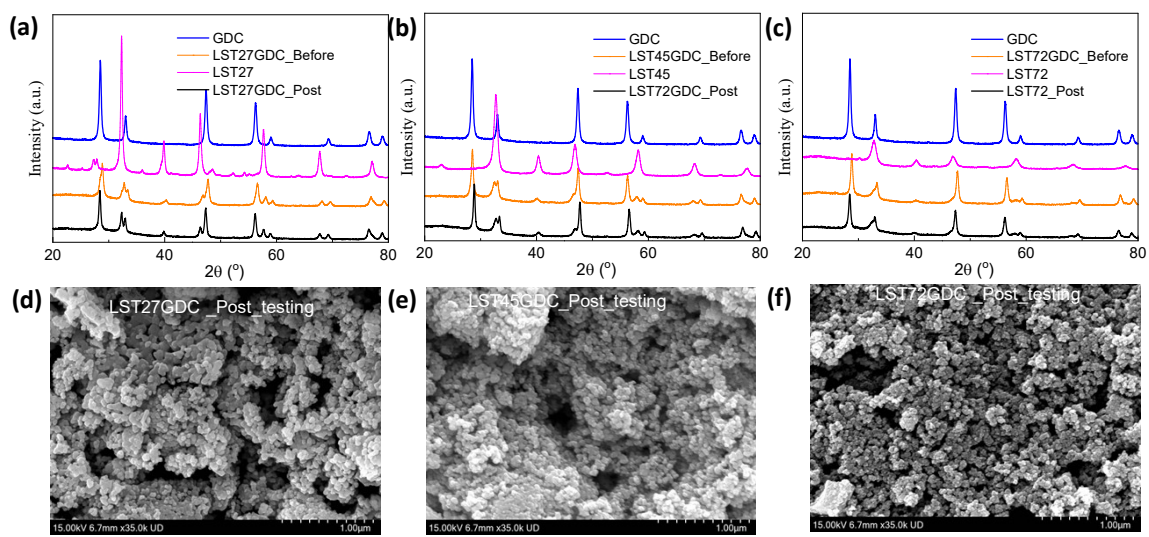


Fig. S4 XRD patters of the samples before testing (a) LST27; (b) LST45 and (c) LST72, SEM images post testing (d) LST27GDC; (e) LST45GDC; (f) LST72GDC.

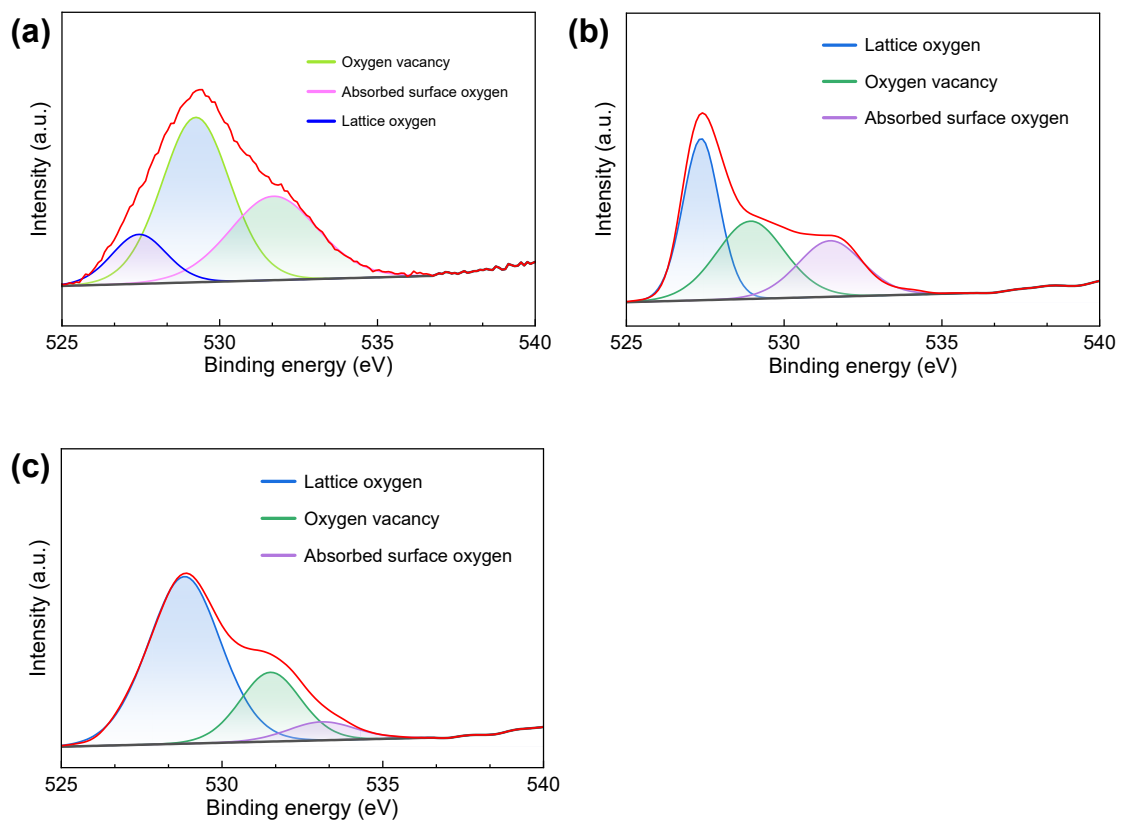


Fig. S5 O_{1s}XPS spectra of (a) LST27 after methane coupling; (b) LST45 after methane coupling; (c) LST72 after methane coupling.

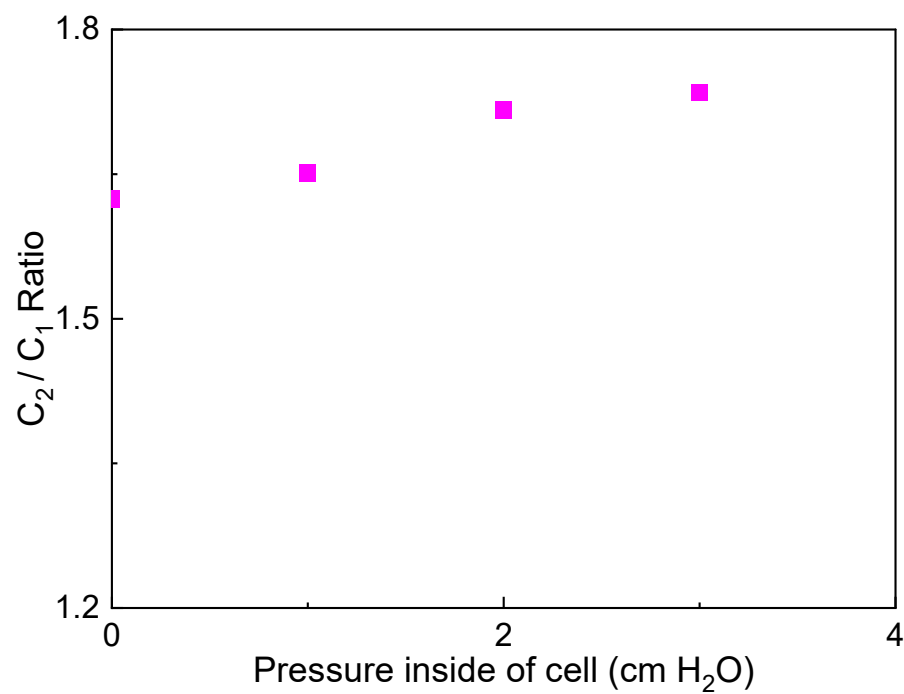


Fig. S6 C_2/C_1 ratio as a function of positive pressure inside of anode chamber ($\text{cm H}_2\text{O}$), 100ml/m air and 50ml/m CH_4 at 0 current.

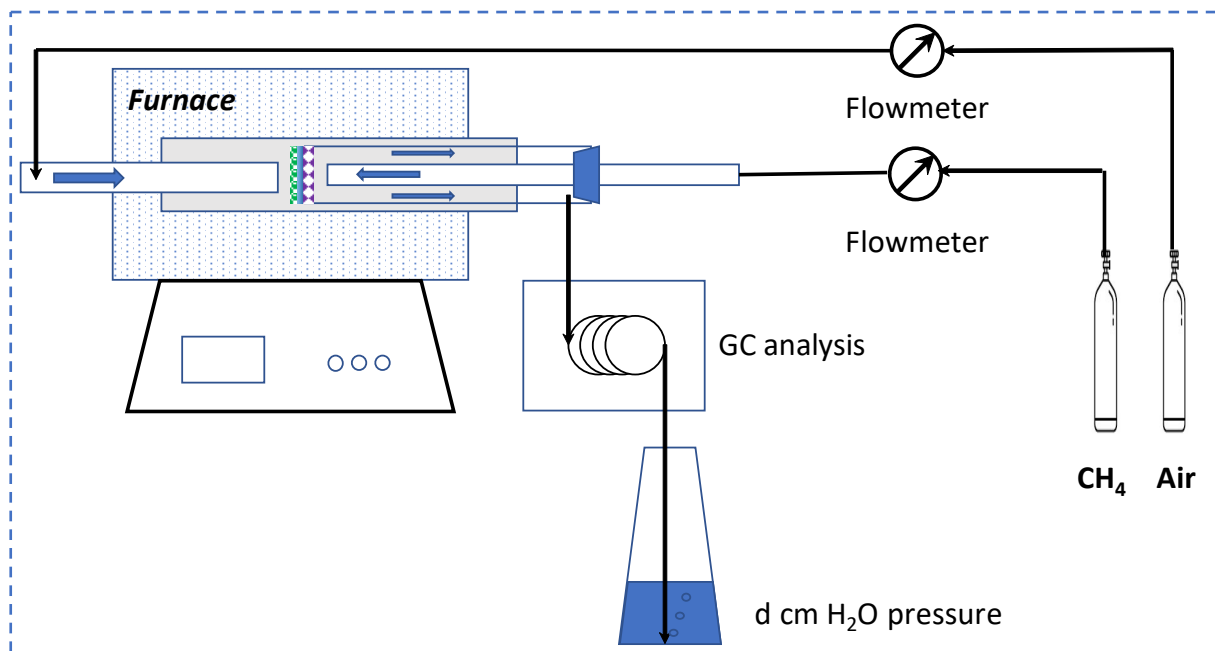


Fig. S7 Schematic of the experimental setup.

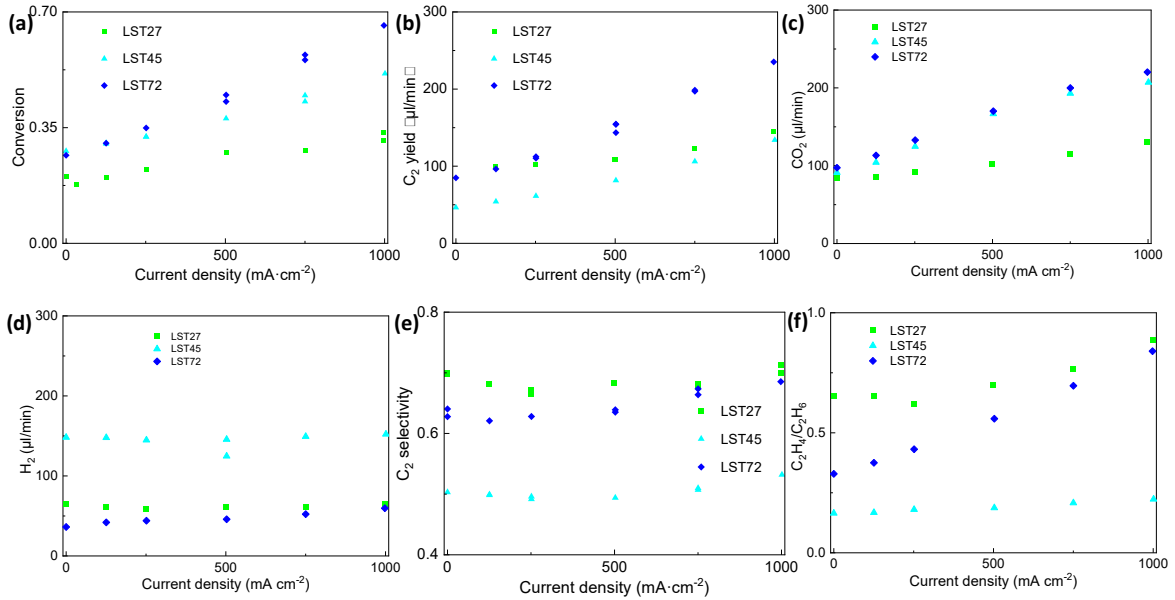


Fig. S8 Catalytic performance for methane conversion using a SOFC button cell design (a) C_2 concentration, (b) CO_2 concentration, (c) H_2 concentration, (d) $\text{C}_2\text{H}_4/\text{C}_2\text{H}_6$ and (e) C_2 selectivity and (f) methane conversion% as a function of current density.

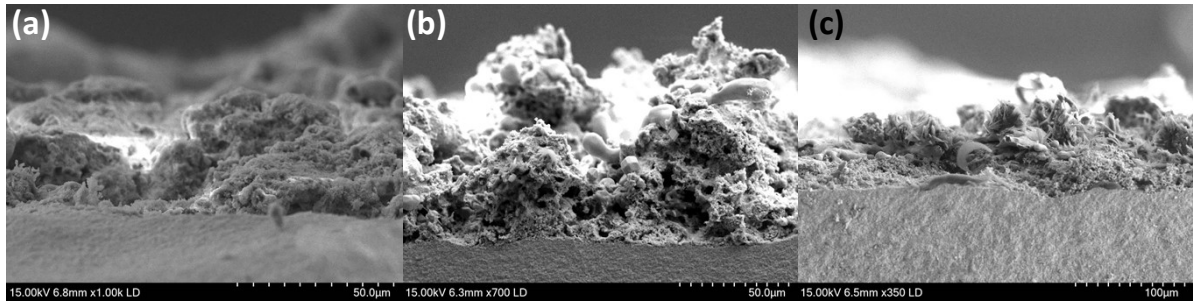


Fig. S9 Cross-sectional images of (a) LST27GDC/GDC, (b) LST45GDC/GDC and (c) LST72GDC/GDC.

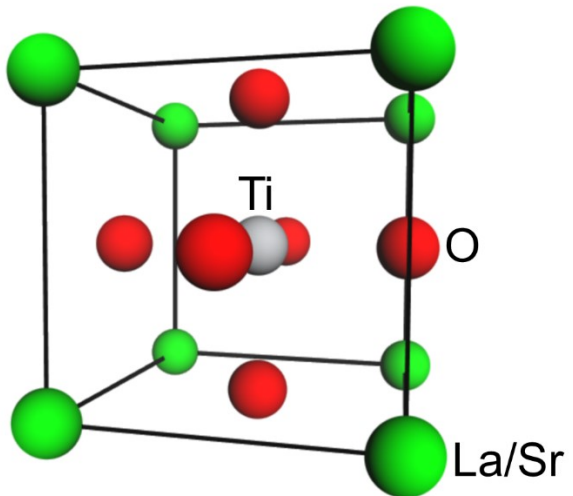


Fig. S10. Crystal structure employed for computational modeling. The structure is based on SrTiO_3 crystal, in which the Sr positions are replaced by La in different proportions. La/Sr: large green spheres; Ti: large grey spheres; O: large red spheres.

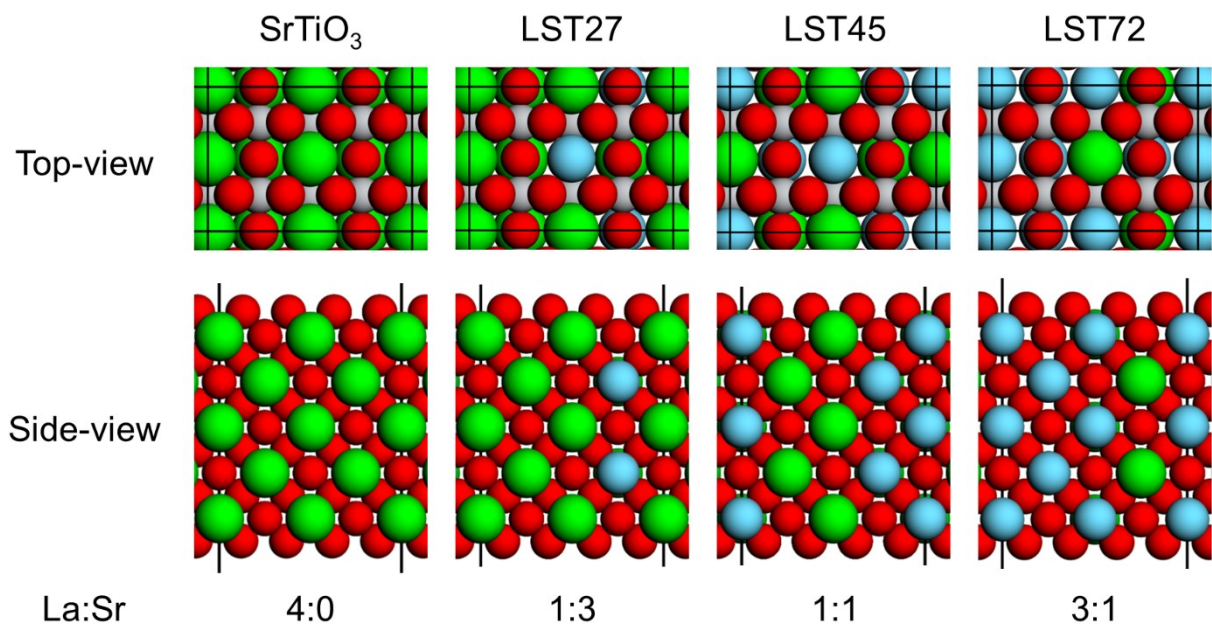


Fig. S11. Computational models of different catalyst surfaces based on $\text{SrTiO}_3(110)$. For the simulation of LST27, LST45, and LST72 catalysts, a symmetric model is employed where each La/Sr layer follows La:Sr ratios of 1:3, 1:1, and 3:1, respectively. La: large blue spheres; Sr: large green spheres; Ti: large grey spheres; O: large red spheres.

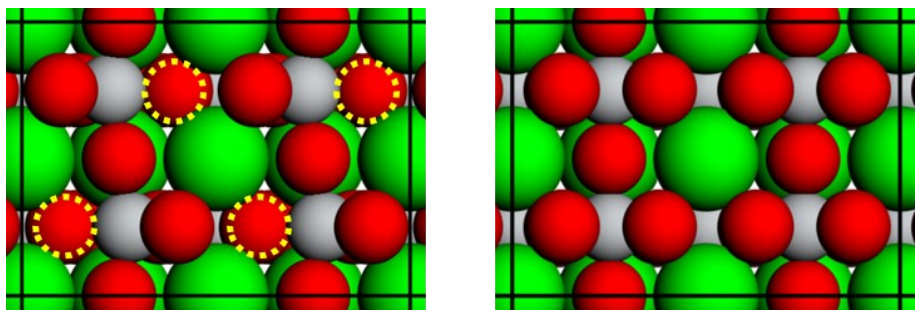


Fig. S12. Surface structures (top view) with (left) and without (right) oxygen (O)-vacancy for calculation of reaction energy (ΔE). The positions of O-vacancies are marked with yellow dotted circles. La/Sr: large green spheres; Ti: large grey spheres; O: large red spheres.